Supplementary Information for:

Tuning inter-dot tunnel coupling of an etched graphene double quantum dot by adjacent metal gates

Da Wei[1], Hai-Ou Li[1], Gang Cao[1], Gang Luo[1], Zhi-Xiong Zheng[1], Tao Tu[1], Ming Xiao[1], Guang-Can Guo[1], Hong-Wen Jiang[2] & Guo-Ping Guo[1*]

1.Key Laboratory of Quantum Information, Department of Optics and Optical Engineering, University of Science and Technology of China, Chinese Academy of Science, Hefei 230026, China.

2.Department of Physics and Astronomy, University of California at Los Angeles, California 90095, USA.

In this supplementary material, we supply technical details including mathematical procedures, sample characterization and an evaluation of all-metal-side-gated samples, which were outlined in the main text:

1. Converting LP (Left Plunger gate) voltage to detuning along the detuning line.

Here, we show the derivation of the conversion relation that turn the FWHM (V) into FWHM (eV) and demonstrate how to achieve such conversion experimentally. This part is solely based on the charge network description of DQD system from ref.16.
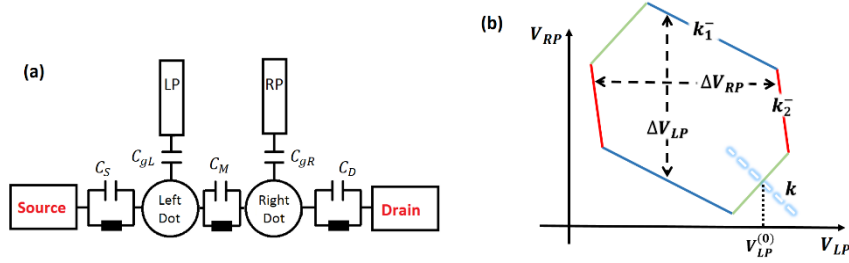
Fig. S1 schematic illustration for device charge network and measured honeycomb structure. (a) A typical charge network model to describe the DQD system we use here [14]. Without loss of generality we omit other gates whose voltage stay fixed when sweeping along the detuning line. (b) The illustration for notations used afterwards in a typical honeycomb. The detuning line is marked with its slope k. k_1^- and k_2^- are slopes of honeycomb edges. ΔV_{LP} and ΔV_{RP} are the size of the comb in each axis.

The electrochemical potential in each dot is:

$$\mu_L(M, N, V_{LP}, V_{RP}) = \left(M - \frac{1}{2}\right)E_{cL} + NE_{cM} - \frac{1}{|e|}(C_{gL}E_{cL}V_{LP} + C_{gR}E_{cM}V_{RP}) \tag{S1}$$

$$\mu_R(M, N, V_{LP}, V_{RP}) = ME_{cM} + \left(N - \frac{1}{2}\right)E_{cR} - \frac{1}{|e|}(C_{gL}E_{cM}V_{LP} + C_{gR}E_{cR}V_{RP}) \tag{S2}$$

$$E_{cL} = \frac{C_R}{C_L C_R - C_M^2}e^2, \ E_{cR} = \frac{C_L}{C_L C_R - C_M^2}e^2, \ E_{cM} = \frac{C_M}{C_L C_R - C_M^2}e^2 \tag{S3}$$

$\mu_{R(L)}(M, N, V_{LP}, V_{RP})$ describes the electrochemical potential needed for adding the Nth (Mth) electron into the right (left) dot with left (right) dot containing M(N) electrons and V_{LP} and V_{RP} applying to the plunger gates respectively. $C_{L(R)}$ is the total capacitance of left (right) dot. $|e|$ is the absolute value of the elementary charge unit.

Define the detuning ε, as $\varepsilon = \mu_L - \mu_R$. We obtain:

$$\varepsilon = -(V_{LP} - V_{LP}^{(0)}) \cdot [\frac{C_{gL}(C_R - C_M)}{C_L C_R - C_M^2}] \cdot (1 + k^2) \tag{S4}$$

Which is the theoretical conversion relation eq. (3). However, experimentally the C_L, C_R and C_M cannot be obtained directly from honeycomb diagram. Thus, we take advantage of handy quantities such as $k_{1(2)}^-$, k and $\Delta V_{LP(RP)}$ from the honeycombs instead.

From eq.(S1) and eq.(S2), one can obtain:

$$k_1^- = -\frac{C_{gL}}{C_{gR}} \cdot \frac{C_M}{C_L} \tag{S5}$$

$$k_2^- = -\frac{C_{gL}}{C_{gR}} \cdot \frac{C_R}{C_M} \tag{S6}$$

$$\Delta V_{LP(RP)} = \frac{|e|}{C_{gL(gR)}} \tag{S7}$$

After substitution, we may obtain the practical form of the conversion relation:

$$\varepsilon = -(V_{LP} - V_{LP}^{(0)}) \cdot \left[\frac{\alpha_L \cdot (1 + \frac{\Delta V_{RP}}{\Delta V_{LP}} \cdot \frac{1}{k_2^-})}{(1 - \frac{k_1^-}{k_2^-})}\right] \cdot (1 + k^2) \tag{S8}$$

Where $\alpha_L = C_{gL}/C_L$ and can be extract accurately through the electron temperature measuring experiment described in the main text.

2. Deduction of the relation between transition peak width FWHM (eV), electron temperature T_e and tunneling coupling strength t_C

The deduction of the relation that connects FWHM (eV), T_e, and t_C altogether- eq.(1) in the main text, is solely based on a well-examined model in ref. 3. Here, we modified it for our transconductance measurement.

In the following text the FWHM (eV) stands for peak width in unit of detuning, T_e for electron temperature and t_C for tunneling coupling strength.

The mathematical description of the conductance of QPC sensor is [3]:

$$G_{QPC}(\varepsilon) = G_0 + \delta G \frac{\varepsilon}{\Omega} th\left(\frac{\Omega}{2k_B T_e}\right) + \frac{\partial G}{\partial \varepsilon}\varepsilon; \; with \; \Omega = \sqrt{\varepsilon^2 + t_C^2} \tag{S9}$$

G_0, δG and $\partial G/\partial \varepsilon$ are the background conductance of the sensor, the sensor sensitivity,

and the direct gate-QPC coupling respectively. As the detuning range that we employed to

investigate the transition peak width is small enough, they can all be considered as constants.

Thus, after take derivative with respect to ε, the transconductance, G_{trans} will mimic the

shape of:

$$A + B\left[\frac{t_C^2}{2\Omega^3} th\left(\frac{\Omega}{2k_B T_e}\right) + \frac{\varepsilon^2}{2\Omega^3}\frac{1}{ch^2\left(\frac{\Omega}{2k_B T_e}\right)}\right] \tag{S10}$$

A and B are constants here. As $(t_C^2/2\Omega^3)\,th(\Omega/2k_B T_e) + (\varepsilon^2/2\Omega^3)ch^{-2}(\Omega/2k_B T_e)$ is a

symmetric peak function centering at $\varepsilon = 0$, whose width has nothing to do with A or B, we may

normalize the G_{trans} by setting A=0 and B=1, then G_{trans}^{norm} writes:

$$G_{trans}^{norm}(\varepsilon) = \left[\frac{t_C^2}{2\Omega^3} th\left(\frac{\Omega}{2k_B T_e}\right) + \frac{\varepsilon^2}{2\Omega^3}\frac{1}{ch^2\left(\frac{\Omega}{2k_B T_e}\right)}\right] \tag{S11}$$

The distance between two solutions for $G_{trans}^{norm}(\varepsilon)$=1/2 is the FWHM (eV).

Symmetry with respect to $\varepsilon = 0$ within $G_{trans}^{norm}(\varepsilon)$ gives:

$$G_{trans}^{norm}\left(\frac{FWHM(eV)}{2}\right) = \frac{1}{2} \tag{S12}$$

To simplify the form of eq.(S12), we may denote:

$$F = \frac{FWHM\,(eV)}{2}\cdot\frac{1}{2k_B T_e}; \Delta = \frac{t_C}{2k_B T_e}. \tag{S13}$$

Thus, we eventually obtain eq.(1) in the main text:

$$\frac{\Delta^2}{\sqrt{\Delta^2+F^2}^3} th\left(\sqrt{\Delta^2 + F^2}\right) + \frac{F^2}{\Delta^2+F^2} ch^{-2}\left(\sqrt{\Delta^2 + F^2}\right) = \frac{th\Delta}{2\Delta} \tag{S15}$$

When T_e and t_C satisfy $t_C \ll 2k_B T_e$, that is, $\Delta \ll 1$, eq. (S15) will become:

$$F \approx \ln(\sqrt{2} + 1) \tag{S16}$$

This indicates that FWHM (eV) will depend linearly on T_e, which is eq.(2) in the main text.

3. Sample characterization

The devices tested here are graphene sheets of 1~2 layers on substrates of 100nm oxide heavily doped silicon chip/ 300nm oxide non-doped silicon chip.

As for ones on heavily doped substrate, the doped substrate works as a back gate that can tune the Fermi level of the whole graphene sheet. On average, the conventional transport gap in unit of back gate voltage is about 10V, energetically, ~1eV. The charging energy of each dot is ~1meV to ~5meV.

The samples without back gate can form quantum dot without of back gate tuning.

The major data presented in the main text are from samples on 100nm oxide heavily doped silicon chip working in hole-doped regime as the red box marked in figure S2.
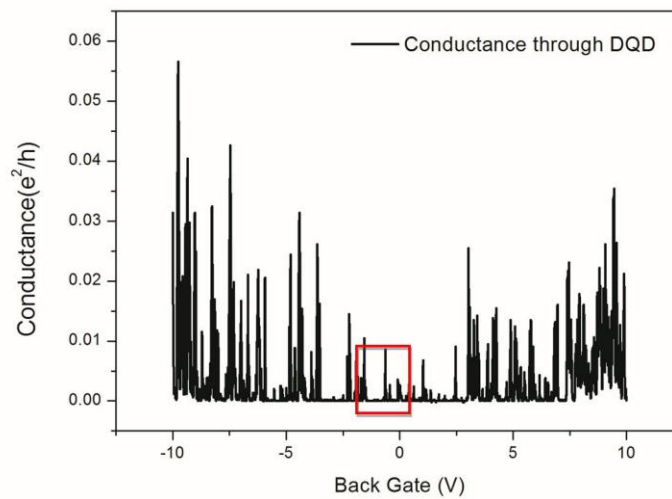
Fig. S2. Measurement of sample conductance vs. back gate voltage. For the bulk of the data presented in the main text, the back gate works in regime marked by red box

in the graph. The transport gap differs from sample to sample though they are designed to be identical and fabricated through same procedure. For such designed samples, transport gaps are of sizes from 6V to 15V, with an average gap size of ~10V.

4. All-metal-side-gated sample performance.

We study the tuning effect of t_C by electron number in one dot in over 10 samples. Such tunability are estimated majorly from QPC sensing measurement, direct transport measurement and superconducting cavity sensing is also used as supplementary measures.

With great care, we have measured the electron temperature (T_e) and corresponding lever arm (α) in the sample presented in the main text, meanwhile, for the other QPC-sensed samples, T_e and α are only roughly estimated, resulting in a relatively large error in the absolute t_C value. However, as T_e and α will only modify the set of data as a whole, the study of t_C monotonicity and tunability still holds.

The monotonic trend in t_C's dependence on electron number is found to survive on average about 5 electrons as shown in figure S3. The t_C tunability for each monotonic trend ranges from a factor of 2 to a factor of 5. t_C ranging from ~10μeV to ~500μeV is observed in different gating configuration.

The longest monotonic trend survive more than 10 electrons meanwhile the commonly observed ones are about 5 electrons. No obvious difference between samples of different substrate is observed. Within the monotonic tuning area, through adjusting the middle gate voltage, t_C can also be tuned.
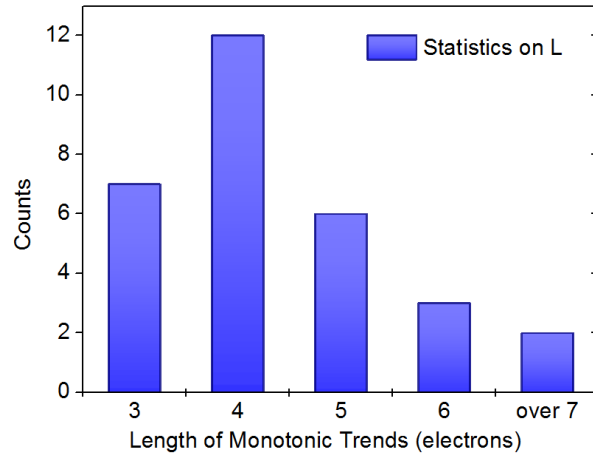
Fig. S3. Statistics on how long do the monotonic dependencies of t_c on electron number in one dot last; L is defined as such length in unit of electron numbers. Throughout all the sample tested, t_c's dependence on electron number in left /right dot (columns/rows of inter-dot charge transition lines in the honeycomb diagram) is investigated. Those columns and rows are selected randomly from regions of regular shaped honeycombs. Note that L is counted without discriminating data obtained from different samples or between columns and rows.

Admittedly, to accomplish a perfect "control" experiment, more samples of identical structure with graphene serving as side gate terminals should be investigated to substantiate the similar statistics as shown in figure S3. However, as we firstly tested 3 samples with graphene gate terminal, the region size demonstrating finely-shaped honeycombs are limited and thus not sufficient to study electron number's effects on t_c.

Through carefully tuning, in such samples, regions consisting of about 5×5 honeycombs could be found, however, from our points of view, such areas are not well-qualified to represent

the sample performance. After the all-metal-side-gated technique is applied, the typical size of finely-shaped region is about 10×10. In some specific samples, such region may even contain 50×50 finely-shaped honeycombs.
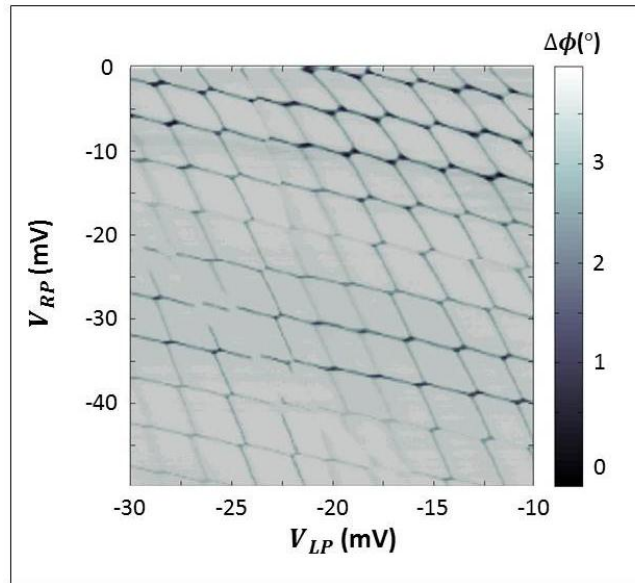
Fig. S4. Typical finely shaped region (10×10) in all-metal-side-gated samples. Standard superconducting probing technique instead of QPC sensing is applied to avoid signal being compromised by background fluctuation [Ref. S1-S4].

Here we cannot rule out the possibility that the sample cleanness (graphene sheet cleanness including the amounts of adsorbed molecules, glue residues, etc.) have also contributed to the fine performance of the all-metal-side-gated samples. Due to the fact that such statistics is quite time-consuming, we cannot afford testing more traditional samples. A quantitative study of the traditional samples which will bring about more statistics are thus called for.

Based on those facts, together with experimental experiences that narrow graphene ribbon will spontaneously form quantum dot, we speculate that the all-metal-side-gated fabrication technique is helpful to enhance the sample performance.

The etch-defined samples presented in literature so far have gate terminals ranging from 50nm to 100nm, for such width, the crippled performance of graphene serving as gate terminals may still be underwater, nevertheless, as device size becoming smaller, leads becoming finer, the advantage of all-metal-side-gated sample will be more and more obvious.

Reference:

[S1] Petersson, K. D. et al. Circuit quantum electrodynamics with a spin qubit. *Nature.* **490,** 380-383 (2012).

[S2] Frey, T. et al. Dipole coupling of a double quantum dot to a microwave resonator. *P.R.L.* **180,** 046807 (2012).

[S3] Toida, H. et al. Vacuum rabi splitting in a semiconductor circuit QED system. *P.R.L.* **110,** 066802 (2013).

[S4] Basset, J. et al. Exploring the Single-Electron Regime of a Double Quantum Dot in the Circuit Quantum Electrodynamics Architecture. *arXiv:***1304**.5141 (2013).